



**HAL**  
open science

## **Fine-scale study of a thick stratospheric ozone lamina at the edge of the southern subtropical barrier: 2.**

### **Numerical simulations with coupled dynamics models**

Béatrice Morel, Hassan Bencherif, Philippe Keckhut, Thierry Portafaix, Alain Hauchecorne, Serge Baldy

► **To cite this version:**

Béatrice Morel, Hassan Bencherif, Philippe Keckhut, Thierry Portafaix, Alain Hauchecorne, et al.. Fine-scale study of a thick stratospheric ozone lamina at the edge of the southern subtropical barrier: 2. Numerical simulations with coupled dynamics models. *Journal of Geophysical Research: Atmospheres*, 2005, 110 (17), pp.D17101. 10.1029/2004JD005737 . hal-00068745

**HAL Id: hal-00068745**

**<https://hal.science/hal-00068745>**

Submitted on 21 Jan 2016

**HAL** is a multi-disciplinary open access archive for the deposit and dissemination of scientific research documents, whether they are published or not. The documents may come from teaching and research institutions in France or abroad, or from public or private research centers.

L'archive ouverte pluridisciplinaire **HAL**, est destinée au dépôt et à la diffusion de documents scientifiques de niveau recherche, publiés ou non, émanant des établissements d'enseignement et de recherche français ou étrangers, des laboratoires publics ou privés.

## Fine-scale study of a thick stratospheric ozone lamina at the edge of the southern subtropical barrier:

### 2. Numerical simulations with coupled dynamics models

Béatrice Morel,<sup>1</sup> Hassan Bencherif,<sup>1</sup> Philippe Keckhut,<sup>2</sup> Thierry Portafaix,<sup>1</sup> Alain Hauchecorne,<sup>2</sup> and Serge Baldy<sup>1</sup>

Received 23 December 2004; revised 29 April 2005; accepted 8 June 2005; published 2 September 2005.

[1] The modeling of an event such as an ozone lamina requires reproducing both the global and the small scales. In this study we report on a specific model capable of resolving such scale issues: the COMMID model, which has been developed by coupling a mechanistic model, MSDOL, with a high-resolution advection model, MIMOSA. MSDOL, which is forced toward National Centers for Environmental Prediction (NCEP) reanalyses below 100 hPa, provides a consistent picture of the stratospheric large-scale circulation from which MIMOSA simulates the fine-scale filaments generated by breaking planetary waves in the stratosphere. To evaluate the performances of the model, we present results for a particular event of tropical-air intrusion at midlatitudes across the southern subtropical barrier observed in July 2000 and described in part 1 (Portafaix et al., 2003). The model is used to examine the contribution of each wave to the structure and the development of that event. The methodology consists in filtering the NCEP tropospheric forcing by zonal wave number and by phase speed. Our results show that mixing is significantly reduced precisely at the locations where the phase speeds of the filtered waves are close to the speed of the mean zonal wind, thus confirming the findings of previous studies. However, what is important here is that they validate the use of an approach based on the coupling of two models. The next step will consist in using the COMMID model in a more general way for further investigations of the impact of the tropospheric circulation on the isentropic transport in the stratosphere for climate sensitivity purposes.

**Citation:** Morel, B., H. Bencherif, P. Keckhut, T. Portafaix, A. Hauchecorne, and S. Baldy (2005), Fine-scale study of a thick stratospheric ozone lamina at the edge of the southern subtropical barrier: 2. Numerical simulations with coupled dynamics models, *J. Geophys. Res.*, 110, D17101, doi:10.1029/2004JD005737.

### 1. Introduction

[2] Over the last 10 years, there has been increasing recognition of the heterogeneous nature of stratospheric transport and mixing. A summary of the main points relevant to stratospheric transport is made by *Plumb* [2002]. It is now widely recognized that the stratosphere is divided into regions of rapid isentropic stirring separated by barrier regions in which stirring is weak and across which there is no, or relatively little, transport. Some studies have been associated with the polar-vortex edge barrier [e.g., *Waugh et al.*, 1994a; *Bowman*, 1996], and others with the subtropical barrier [e.g., *Randel et al.*, 1993; *Chen et al.*, 1994; *Waugh et al.*, 1994b; *Bowman and Hu*, 1997; *Bencherif et al.*, 2003; *Portafaix et al.*, 2003].

Isentropic exchange of stratospheric air across those barriers has been a subject of considerable interest recently, in particular, by attribution of some of the observed trends in midlatitude ozone to the isentropic transport of polar air toward midlatitudes [*Hauchecorne et al.*, 2001; *U.N. Environment Programme/World Meteorological Organization (UNEP/WMO)*, 2002]. It is now well recognized that such exchange is controlled by Rossby-wave breaking in the surf zone [*McIntyre and Palmer*, 1984]. Although an overall understanding of how it works has been established, a number of details remain unclear and need to be sorted out in order to obtain reliable estimates of cross-barrier mass transport and to improve its representation in climatic models for long-term climate simulations.

[3] Rossby-wave breaking is typically characterized by the irreversible deformation of potential-vorticity (PV) contours on isentropic surfaces and the subsequent mixing of different air masses. The nature of the breaking is consistent with the predictions of the Rossby-wave critical-layer theory [*Stewartson*, 1978; *Warn and Warn*, 1978; *Haynes*, 2003]: As Rossby waves propagate upward from the troposphere through wintertime stratospheric westerlies, their

<sup>1</sup>Laboratoire de Physique de l'Atmosphère, Université de La Réunion, La Réunion, France.

<sup>2</sup>Service d'Aéronomie, Institut Pierre-Simon Laplace–CNRS, Verrières-le Buisson, France.

amplitude increases [Andrews *et al.*, 1987]; at sufficiently large amplitude, the waves break on reaching critical lines where they become stationary with respect to the flow field. The presence of the mixing barriers in the stratosphere is also well explained by the critical-layer framework. Using unfiltered and filtered stratospheric winds, Bowman [1996] and Bowman and Hu [1997] tested the relationship between wave phase speeds and mixing barriers.

[4] One of the most important issues in understanding the transport in the Upper Troposphere/Lower Stratosphere (UTLS) is an understanding of the climatic chemical-radiative-dynamical feedbacks in the system. For that reason, climate modeling requires careful attention of the UTLS region and, especially, the tropical tropopause layer it includes. Because isentropic transport and mixing processes in the UTLS operate on scales from hundreds to thousands of kilometers, the challenge then is to develop numerical tools capable of resolving scale issues that allow climate sensitivity studies as well as statistical studies. In this study, we report on such a model: the COupled Mimosa Msdol Interactive Dynamics (COMMID) model, in which the tropospheric component has been removed, and which then allows us to prescribe the tropospheric dynamical forcing. This model is the first step toward the development of a more complex/detailed model that will involve a general circulation model [Lott *et al.*, 2005] for full simulations of the UTLS region. The COMMID model will be used to investigate the impact of the tropospheric circulation on the isentropic transport in the stratosphere. Since the tropospheric circulation in the model can be prescribed, it will allow us to better understand the origin of the stratospheric changes.

[5] The objective here is to present the results for a case study to evaluate the performances of the model. The case study that has been selected is a large-scale isentropic transport event near the southern subtropical barrier observed in July 2000, and which is well documented in part 1 [Portafaix *et al.*, 2003] (hereinafter referred to as P03). In this paper we first verify that the COMMID model is able to realistically simulate that event. We then examine the role of different parts of the wave spectrum on mixing by selectively forcing waves in the troposphere. The paper is organized as follows. In section 2, we describe the COMMID model and the methods and diagnostics used throughout the remainder of the paper. The COMMID results for the simulation of the July 2000 event are given in section 3. Section 4 presents a sensitivity study based on the specification of the tropospheric forcing through several case scenarios. A summary is given and conclusions are drawn in section 5.

## 2. Methodology

### 2.1. Model Description

[6] Simulations here are made with the COMMID model which is a combination of the MSDOL (Monitoring of Stratospheric Depletion of Ozone Layer) global 3-D mechanistic model and the MIMOSA (Modélisation Isentrope du transport Méso-échelle de l'Ozone Stratosphérique par Advection) high-resolution advection contour model. The MSDOL model, which is limited to the stratosphere, gives a consistent picture of the evolution of the stratospheric large-

scale circulation through external tropospheric forcing provided by the reanalyses of NCEP. The MIMOSA model is forced by MSDOL fields to simulate the fine-scale filaments generated by breaking planetary waves in the stratosphere.

#### 2.1.1. MSDOL Model

[7] The MSDOL model is based on the ROSE (Research on Ozone in the Stratosphere and its Evolution) dynamical chemical mechanistic model [Rose and Brasseur, 1989], and has been described in detail by Morel *et al.* [2004]. In this study, MSDOL is used to simulate dynamical processes only in the middle atmosphere (10–80 km); chemical fields are specified. Basically, the model solves the 3-D primitive equations in flux form on a sphere with resolution of 11.25° in longitude, 5° in latitude and about 3 km in altitude. It contains parameterisations of radiation calculating solar heating due to O<sub>3</sub> and O<sub>2</sub> absorption and CO<sub>2</sub> infrared cooling. The effects of unresolved gravity waves are also parameterized after Fritts and Lu [1993]. To give realistic wave forcing from the troposphere, horizontal wind, temperature, and geopotential fields below 100 hPa are nudged to daily NCEP reanalyses. In the present study, the MSDOL model is run for 3 months starting on 1 May 2000. Variables are saved every 6 hours. Horizontal winds and temperature are interpolated onto isentropic surfaces.

#### 2.1.2. MIMOSA Model

[8] The MIMOSA high-resolution advection model of PV was developed at Service d'Aéronomie by Hauchecorne *et al.* [2002]. MIMOSA runs on an isentropic surface and two domains centered onto the North and South poles (covering latitudes from 90°N to 10°S and 90°S to 10°N, respectively) with resolution of 3 points per degree; the fields produced for each hemisphere are then linked together within a latitude band of 5° width centred over the equator. The MIMOSA model advects PV fields (computed internally from MSDOL horizontal wind and temperature fields) with a time step of 1 hour by the wind field from MSDOL. To preserve the homogeneity of the field, a regridding of the advected PV field onto the original grid is made every 6 hours. The diabatic evolution of the PV field at large scales can be extracted from MSDOL fields. In MIMOSA, this is made by applying a relaxation toward the MSDOL PV field with a time constant of 10 days. Using this procedure, it is possible to run continuously the model and to follow the evolution of filaments during several months.

## 2.2. Diagnosis Tool

[9] In P03, the subtropical barrier was investigated using the DYBAL (DYnamical BARRIER Localisation) code which combines the equivalent length of a  $q$  contour,  $L_e$ , and the derivative of  $q$  with respect to area  $A$  enclosed by the contour,  $\partial q/\partial A$  [Nakamura, 1996]. Here the transport and mixing properties of the isentropic flow are investigated using the effective diffusivity  $\kappa_{eff}$  [Nakamura and Ma, 1997; Haynes and Shuckburgh, 2000; Hauchecorne *et al.*, 2002] which is related to the squared equivalent length

$$\kappa_{eff} = \frac{\kappa \langle |\nabla q|^2 \rangle}{(\partial q/\partial A)^2} = \kappa L_e^2. \quad (1)$$

Here  $\langle ( ) \rangle$  is the average over the area between adjacent contours, and  $\kappa$  is the local diffusivity. The effective

**Table 1.** Summary of the Simulations

Run identifier	NCEP tropospheric dynamical forcing		Description
	Zonal wave number range	Phase speed range (m/s)	
1	$1 \leq s < \infty$	$-\infty < c < \infty$	control experiment: model run with unfiltered NCEP data
2	$1 \leq s < 4$	$-\infty < c < \infty$	same as run 1, but with NCEP data filtered by zonal wave number $s$
3	$3 < s < \infty$	$-\infty < c < \infty$	
4	$s = 1$	$-\infty < c < \infty$	
5	$s = 2$	$-\infty < c < \infty$	
6	$s = 3$	$-\infty < c < \infty$	
7	$s = 1;2$	$-\infty < c < \infty$	
8	$s = 1;3$	$-\infty < c < \infty$	
9	$s = 2;3$	$-\infty < c < \infty$	
10	$1 \leq s < \infty$	$-\infty < c \leq 20$	
11	$1 \leq s < \infty$	$-\infty < c \leq 10$	
12	$1 \leq s < \infty$	$-\infty < c \leq 5$	
13	$1 \leq s < \infty$	$-\infty < c \leq 0$	
14	$1 \leq s < \infty$	$0 \leq c < \infty$	
15	$1 \leq s < \infty$	$-5 \leq c < \infty$	
16	$1 \leq s < \infty$	$-10 \leq c < \infty$	
17	$1 \leq s < \infty$	$-20 \leq c < \infty$	
18	$1 \leq s < \infty$	$5 \leq  c  < \infty$	
19	$1 \leq s < \infty$	$10 \leq  c  < \infty$	

diffusivity is larger where the tracer contours are longer, i.e., where their geometric structure is more complex. Therefore mixing barriers and regions of large mixing can be identified by relative minima and maxima in the effective diffusivity, respectively.

[10] To estimate  $\kappa_{eff}$ , we first compute PV on an isentropic surface by using horizontal wind and temperature fields provided by MSDOL. We then advect this PV distribution with the aid of MIMOSA. Finally, we calculate  $\kappa_{eff}$  associated with the PV advected by MIMOSA. The effective diffusivity diagnostic has been found to work better to estimate the mixing properties of tracers with the PV advected by MIMOSA than with the “true” PV fields, as the contrast between dynamical barriers and mixing regions is enhanced while maintaining the transport spatial structure of the flow [Hauchecorne *et al.*, 2002]. The reason for that is that the magnitude of effective diffusivity is resolution dependent. In the following, results will be presented in the form of the effective diffusivity  $\kappa_{eff}$  normalized by the local diffusivity  $\kappa$ :  $\tilde{\kappa}_{eff} = \kappa_{eff}/\kappa$ , as a function of equivalent latitude,

$$\phi_e = \arcsin\left(1 - \frac{A}{2\pi a^2}\right), \quad (2)$$

where  $a$  is the Earth’s radius.

### 2.3. Model Simulations

[11] Specifying the planetary-wave forcing from the troposphere using the NCEP data, it is therefore possible to control the amplitude of the forcing and the type of wave it contains. In this study we make a detailed study of the contribution of each wave to an individual isentropic transport event, but rather than filtering the actual stratospheric winds as done by Bowman [1996] and Bowman and Hu [1997], we conduct a series of simulations of the COMMID model with unfiltered and filtered tropospheric forcing (Table 1). The first simulation (run 1) is used as a control run. All other simulations (runs 2 to 19) are used to obtain information about the contribution of each wave on

the structure and the development of the July 2000 event. The approach consists in filtering the tropospheric dynamical forcing provided by the NCEP reanalyses before forcing MSDOL, either in the spatial or the spectral domain [Bowman, 1996]: (1) filtering in the spatial domain to remove waves by zonal wave number  $s$  (runs 2 to 9) by using the fast Fourier transform in the zonal direction and (2) filtering in the spectral domain to remove waves by zonal phase speed  $c$  (runs 10 to 19). The method consists in expanding the NCEP data at each latitude  $\phi$  and on each level  $p$  in a space-time Fourier series as

$$\Psi(\lambda, t) = \sum_s \sum_\omega \psi_{s,\omega} e^{i(s\lambda - \omega t)}, \quad (3)$$

where

- $\Psi$  either the zonal or the meridional component of the horizontal wind, the temperature or the geopotential;
- $\lambda$  longitude;
- $t$  time;
- $s$  discrete spatial frequency (zonal wave number);
- $\omega$  discrete temporal frequency;
- $\psi_{s,\omega}$  complex amplitude of each wave.

The complex 2-D spectrum  $\psi_{s,\omega}$ , which is computed using fast Fourier transforms, is multiplied by a filter depending on the phase speed  $c$  of each traveling wave component:  $c = \omega a(\cos\phi)/s$ . The inverse transform is then computed to produce the filtered horizontal wind, temperature and geopotential fields. The filter acts so as to set to zero the amplitudes of components with phase speeds falling in the range  $c_{min} \leq c \leq c_{max}$ .

[12] In order to determine the most relevant experiments, thus limiting the number of them to conduct, a wave spectrum analysis using NCEP reanalysis for the May–August period has been made to select the filter limits. Results (data not shown) indicate that the largest components in the winter hemisphere during that time period are the stationary and quasi-stationary waves. In general, most

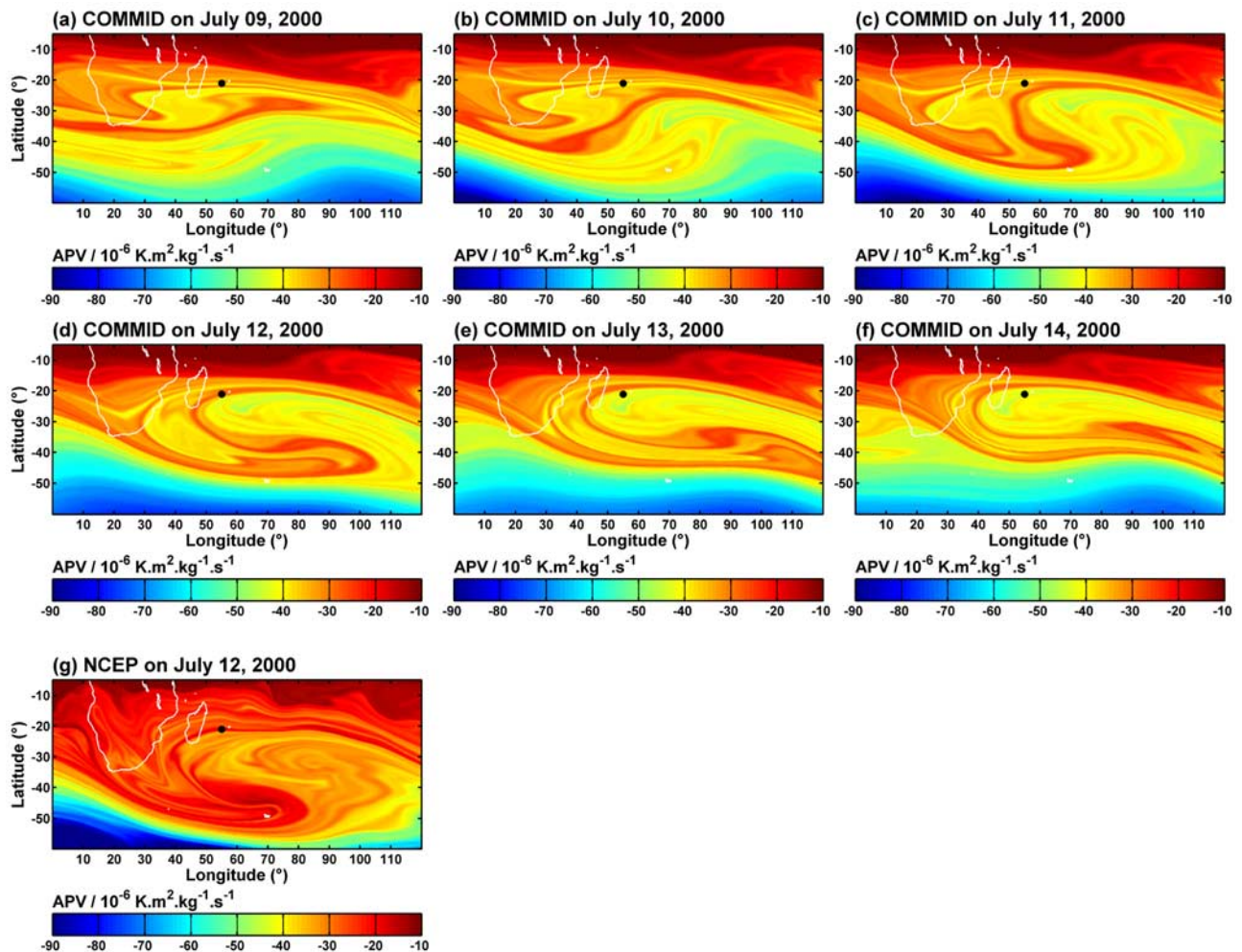


**Figure 1.** Maps of advected PV (APV) at 550 K provided (a–f) by the control simulation of the COMMID model between 9 and 14 July 2000 and (g) by a MIMOSA simulation driven by the NCEP reanalyses on 12 July 2000.

of the waves have phase speeds less than 30 m/s, with power focusing on wave numbers less than 5 and on periods longer than 10 days. In the middle and high latitudes, waves moving eastward have larger power than those moving westward.

### 3. Modeling of the July 2000 Event

#### 3.1. Advected Potential Vorticity

[13] The focus here is to show the ability of the COMMID model to reproduce consistently a large-scale isentropic transport event near the southern subtropical barrier observed in July 2000. This event was investigated and described by P03 from ozone measurements and meteorological analyses provided by the ECMWF analyses. An ozone lamina was seen above Reunion Island ( $21^{\circ}\text{S}$ – $55^{\circ}\text{E}$ ) on 12 July 2000, spanning the isentropic surfaces 550–750 K. Transport of material with midlatitude origin as the cause of this ozone lamina was demonstrated in P03 with the aid of the DYBAL code for identifying barriers and the MIMOSA high-resolution advection model. The transport resulted from the entrainment of a tongue of air from the edge of the tropics into midlatitudes in connection with an episode of planetary-wave breaking.

[14] The evolution of advected PV (APV) on the 550-K isentropic for 9 to 14 July 2000, for the control run of the COMMID model, can be seen in Figures 1a to 1f. It shows the development starting on 9 July of a large tongue of low (absolute value of) APV, which indicates air of tropical origin, stretching southeastward from Southern Africa the next days. Concomitant to this transport is the northward transport of high-PV air from the midlatitudes. Consideration of the time evolution of the wind fields on the 550-K isentropic for the same dates (data not shown) shows that the tongue developed in a region of increasing winds, tilting southeastward on 12 July, and associated with anticyclonic circulation on its northern flank. The motion associated with this intrusion event is similar to that hinted at in the ECMWF analyses (compare Figure 5 of P03). Further, comparison of the APV field for July 12 from the model (Figure 1d) with that provided by a MIMOSA simulation driven by the NCEP reanalyses (Figure 1g) indicates broad agreement of the location of the tongue. Differences are observed, however, in the stretching of the tongue, which extends farther eastward and less poleward in the APV field from the model than from the reanalyses, and in the small scales within it, COMMID giving smoother

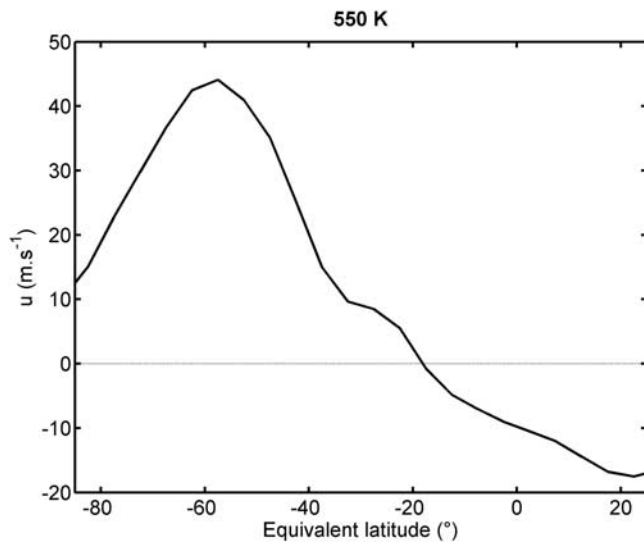


**Figure 2.** Zonal wind as a function of equivalent latitude and averaged over the period 9–16 July 2000, on the 550-K surface, for the control simulation of the COMMID model.

APV contours than NCEP. This may be due to the coarser-grained advecting wind field produced by COMMID [Methven and Hoskins, 1999; Hauchecorne et al., 2002] but not only. Owing to the coarseness of the horizontal grid of the MSDOL model, some waves might not be well resolved. Another possibility is that the amplitude of the waves is badly reproduced by the model. Besides, wave propagation depends on the mean flow while the latter is also affected by the specification of the gravity-wave drag. As regards the mean state of the stratosphere, the MSDOL model underestimates the zonal wind in the upper levels (data not shown), thus leading to differences in the conditions of propagation of the waves. For example, the location of the critical surface corresponding to zero zonal wind, which determines the location for breaking stationary waves, is different between MSDOL and NCEP. Also apparent are the quantitative differences, as for example larger (absolute) values of APV within the tongue from COMMID (Figure 1d) than from NCEP (Figure 1g). This may be related to the PV gradient between the surf zone and the vortex-edge barrier which is much less pronounced in MSDOL than it is in NCEP (data not shown). This effect is likely to be attributed to the lack of resolution of MSDOL which does not allow good representation of the strong PV gradient at the edge of the vortex. As a consequence, the PV is weaker (in absolute value) in NCEP than in MSDOL between 15°S and 50°S, causing quantitative differences in the tongue. The vertical structure (data not shown) shows that the depth of the tongue in the model spans the whole region between 450 and 850 K, thus displaying a larger vertical extension than that in the ECMWF analyses (550 to 750 K; see P03). There again, one possible explanation could be the differences in the PV distribution between MSDOL and ECMWF [Polvani and Saravanan, 2000].

### 3.2. Basic-State Wind Profile and Effective Diffusivity Diagnostic

[15] Figure 2 shows the zonal wind as a function of equivalent latitude on the 550-K surface for the control

simulation of the model. It can be seen that the maximum value ( $\sim 45$  m/s) is reached at 50°S–60°S, corresponding to the stratospheric polar-night jet. In addition, there are easterlies (negative values) northward of 15°S–20°S (within the tropical region).

[16] The mixing behavior on the 550-K isentrope for the period 9–16 July is summarized by estimated effective diffusivity as a function of equivalent latitude in Figure 3 (unfiltered tropospheric forcing, in solid line; the other curves are discussed in section 4 below). The surf zone is clearly evident as the broad band of high  $\kappa_{eff}$  (i.e.,  $\ln \tilde{\kappa}_{eff} \geq 1$ ) in the middle and low latitudes of the Southern Hemisphere. There are also quite high values of  $\kappa_{eff}$  within the polar vortex indicating mixing in there. Finally, the effective diffusivity shows two minima corresponding to barrier regions: the first in the Southern Hemisphere high latitudes corresponding to the vortex-edge barrier, and the second a broader minimum centered in the low latitudes of the Northern Hemisphere associated with the stratospheric tropical reservoir. Similar structures are obtained when using a domain limited in longitude centered over the region where the event occurred (between 0°E and 120°E; data not shown), in spite of differences in the small-scale features; that is, a smoothing effect is introduced by the use of a larger domain. Those structures are also well reproduced at all levels in the stratosphere (data not shown). Comparison of our results with those of Haynes and Shuckburgh [2000] and with those obtained from ECMWF and NCEP (data not shown) indicates that the COMMID model is able to reproduce the regions of strong mixing and barriers in the stratosphere. This reinforces our belief that the effective diffusivity can be used to identify, and to make quantitative comparisons between,

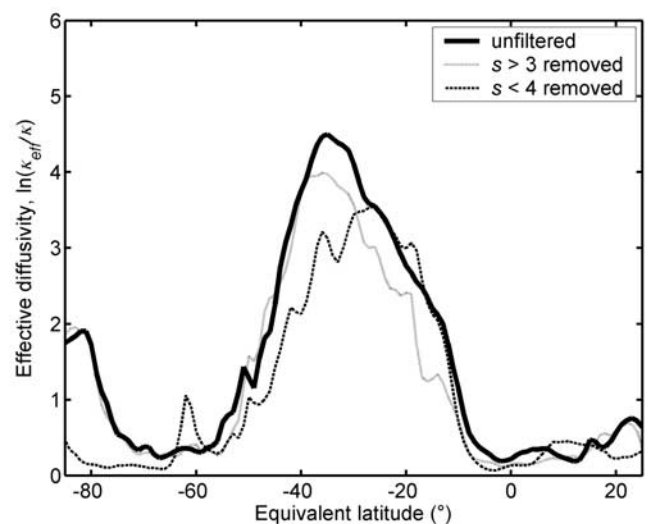


**Figure 3.** Logarithm of normalized  $\kappa_{eff}$  as a function of equivalent latitude and averaged over the period 9–16 July 2000, on the 550-K surface, estimated from the APV fields provided by the COMMID model run with unfiltered NCEP tropospheric dynamical forcing (solid line) and with NCEP tropospheric dynamical forcing filtered by zonal wave number  $s$ :  $s > 3$  removed (dotted line) and  $s < 4$  removed (dashed line).

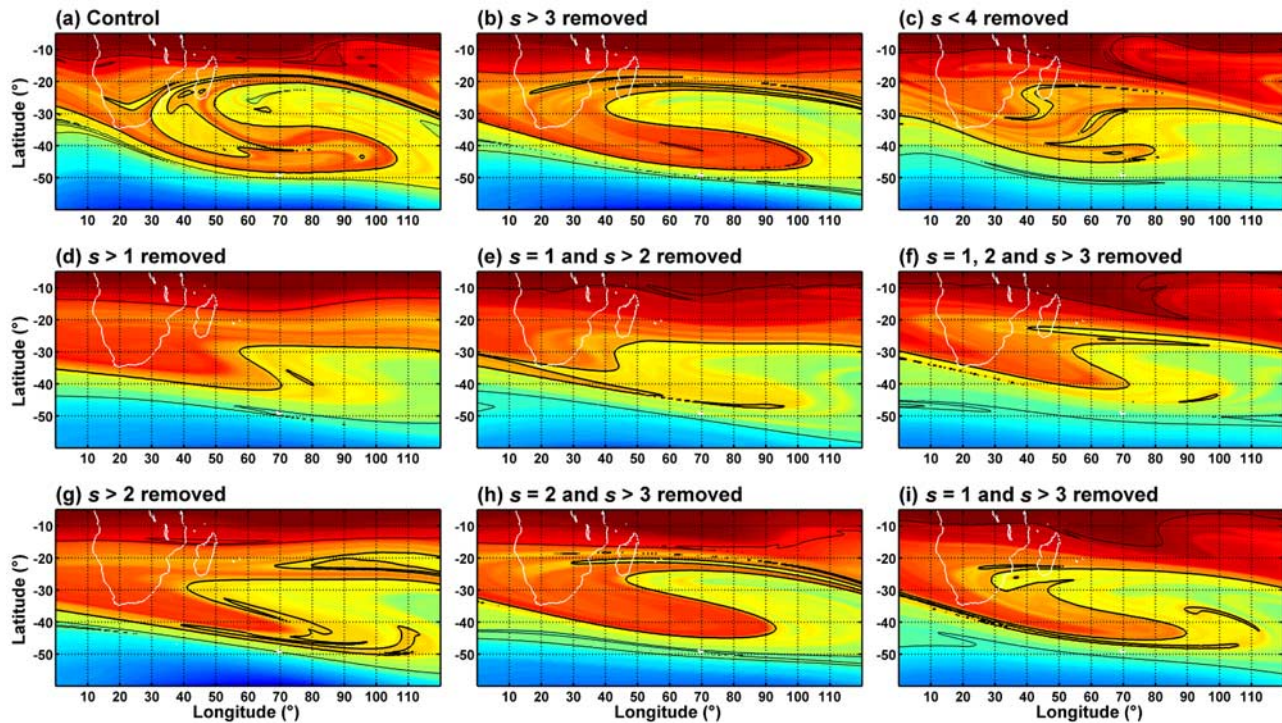


**Figure 4.** As in Figure 1 for several simulations of the COMMID model run with (a) unfiltered NCEP tropospheric dynamical forcing and (b–i) NCEP tropospheric dynamical forcing filtered by zonal wave number  $s$ . The thin contours indicate the edges of the zone of strong mixing (i.e.,  $\ln \tilde{\kappa}_{eff} \geq 1$ ) in the surf zone. The thick black contour represents the  $-37$  PVU iso-APV contour.

transport and mixing regions in selected simulations at differing forcing conditions.

## 4. Sensitivity Tests on the Wave Forcing

### 4.1. Filtering by Zonal Wave Number

[17] Figure 4 shows the APV fields at 550 K on 12 July 2000, for the control run of the COMMID model and for runs with NCEP forcing filtered by zonal wave number. The thin contours that indicate the edges of the zone of strong mixing (i.e., high values of  $\kappa_{eff}$ ) in the surf zone, correspond to the zone in which contours of iso-APV are the most distorted, whereas contours outside of it present quasi-zonal symmetry. All runs show irreversible APV overturning indicating wave breaking, despite differences in morphology. The effects of removing the medium-scale waves can be seen in Figure 4b. In this case, a tropical-air tongue (in red on the figure, and materialized by the thick black contour representing the  $-37$  PVU iso-APV contour) develops above the southwestern basin of the Indian Ocean with nearly the same horizontal extension as that in the control run. Removing the planetary-scale waves (Figure 4c), on the other hand, does not lead to the formation of a clear tongue of low-APV air. From the examination of the APV field for the simulations with all but one planetary mode removed (Figures 4d to 4f), no clear formation of a tongue apart from a bulge that springs up out of Southern Africa and the southwestern basin of the Indian Ocean is apparent either, suggesting that the tongue is generated by the combination of several planetary modes. Three other simulations of the COMMID model

run with all but two planetary modes removed (Figures 4g to 4i) further show that combinations including wave 3 (Figures 4h and 4i) allow to represent the structure of the tongue better. In Figure 4h, it can be seen that the horizontal extension of the tongue is the best reproduced when removing all but waves 1 and 3.

[18] Figure 3 also shows the values of the effective diffusivity from two filters: the first removes the medium-scale waves (dotted line) and the second removes the planetary-scale waves (dashed line). The values of  $\kappa_{eff}$  indicate that mixing is somewhat reduced in the surf zone in both cases. However, the planetary-scale waves are more important in the middle and high latitudes, while the medium-scale waves are more important in the tropics and subtropics. The planetary-scale waves are also more important within the polar vortex, which is probably an effect of the zonal truncation performed at the pole in the MSDOL dynamic iteration loop. Removing all but one planetary mode (data not shown) produces a similar effect, mainly the decrease of the values of  $\kappa_{eff}$  in the surf zone and inside the polar vortex. Whatever the filter, mixing in the surf zone is generally reduced but not eliminated, so it is impossible to attribute the bulk of the mixing to waves with particular spatial scales. This is consistent with results obtained by Bowman [1996] who showed that the large-scale waves are more important at the edge of the polar vortex, but that elsewhere the two wave number bands are roughly equally important. In addition, Chen *et al.* [1994] and Rosenlof *et al.* [1997] reported that the transport in the lower stratosphere is controlled by several factors including forcing by planetary-scale waves and synoptic-scale disturbances.

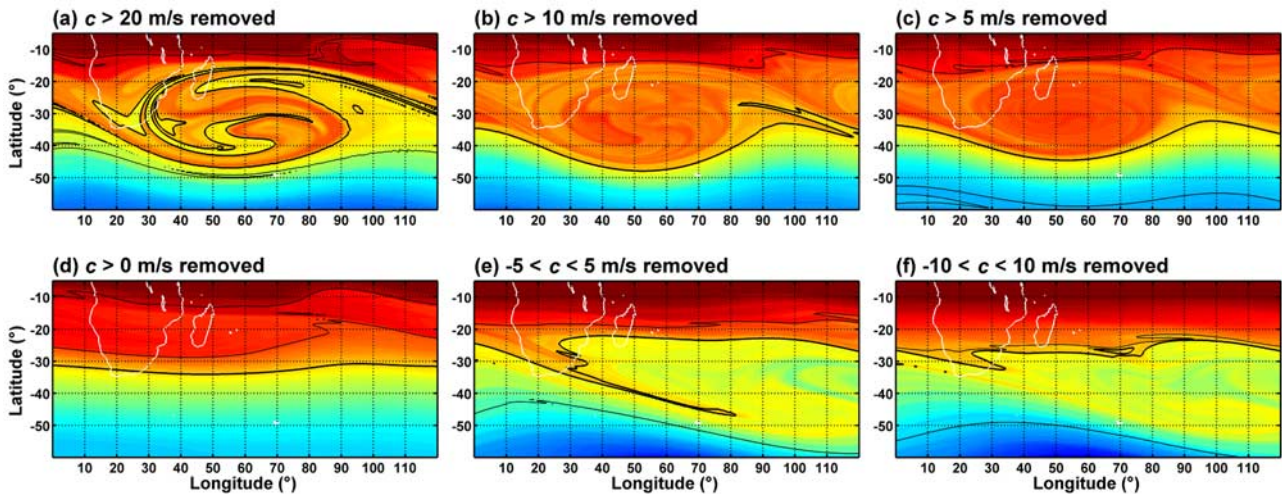


**Figure 5.** As in Figure 4 except that NCEP tropospheric dynamical forcing is filtered by phase speed  $c$ .

#### 4.2. Filtering by Phase Speed

[19] Figure 5 shows the APV fields at 550 K on 12 July 2000, for the control run of the COMMID model and for runs with NCEP forcing filtered by phase speed. Figures 5a to 5d show the low-pass filtered results as the upper limit of the filter is reduced and progressively slower eastward-propagating are removed. The labels indicate the upper cut-off of the low-pass filter. Thus  $c > 20$  m/s indicates that all waves with phase speeds greater than 20 m/s (at  $45^\circ\text{S}$ ) are removed. Figures 5e and 5f show the band-gap filtered results, in which waves with phase speeds between two finite limits are filtered. There again, irreversible APV overturning is seen in all runs shown in Figure 5 but the one with all eastward-propagating waves removed (Figure 5d) in which wave breaking did not occur. In that case, there is no development of a tongue and the mixing is strongly reduced as indicated by the quasi-zonal symmetry of the contours of iso-APV. One reason could be that the region of high wind speeds, which remains whatever the filter, does not tilt in the same way as in the other runs (data not shown). Conversely, APV overturning outside the longitudes plotted is not seen in all simulations. When the slow-propagating waves are filtered (Figures 5e and 5f), there is no clear formation of a tongue either and the mixing decreases much more at the tropical edge of the surf zone. When a larger band-gap of phase speeds is selected (Figure 5f), the tropical edge of the surf zone moves farther southward.

[20] The effective diffusivity for the low-pass and the band-gap filtered NCEP forcing is shown in Figures 6a and 6b, respectively. As in Figure 3, the values of  $\kappa_{\text{eff}}$  from the unfiltered run are plotted for comparison (thick solid line). Figure 6a shows that for almost all filters, mixing is strongly reduced in the polar vortex and in the surf zone. Yet, removing the fastest eastward-propagating waves ( $c > 20$  m/s) has only a small effect on the mixing in the surf zone. Removing slower and slower waves, on the other hand, results in significant changes in the values of  $\kappa_{\text{eff}}$ . Mixing at the vortex edge, where the wind speeds are the highest (Figure 2), is steadily reduced as slower and slower waves are removed, moving the polar edge of the region of

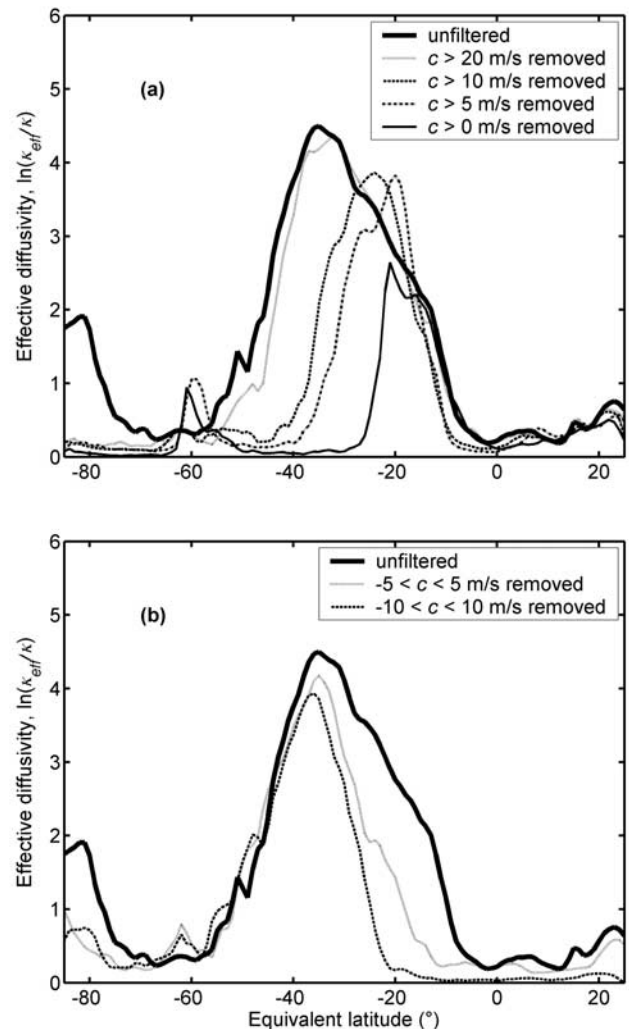


**Figure 6.** As in Figure 3 except that NCEP tropospheric dynamical forcing is filtered by phase speed  $c$ : (a) eastward-moving waves removed and (b) slow-moving waves removed (see text for details).

high values of  $\kappa_{\text{eff}}$  to lower latitude. In the borderline case where all eastward-propagating waves are filtered, there are high values of  $\kappa_{\text{eff}}$  in between 10°S and 25°S only. Given that the eastward-propagating waves represent much of the wave activity propagating vertically from the troposphere into the stratospheric westerlies during winter [Charney and Drazin, 1961], this is not surprising. There are also some changes in the tropics for the runs in which all waves with phase speeds greater than 10 and 5 m/s are removed, especially significant increase in the mixing around 20°S. Finally, whatever the filter, mixing in the tropical stratospheric reservoir is hardly affected at all. Conversely, the westward-propagating waves (data not shown) have much less impact on the mixing, except in the tropical region where filtering the slowest waves reduces mixing, as would be expected with the weak negative values of the zonal wind in that region (Figure 2). The band-gap filters (Figure 6b) result in significant changes in the polar vortex and in the surf zone. Mixing in the surf zone is hardly affected at all at the polar edge. At the tropical edge, on the other hand, the mixing decreases significantly and even further when a larger band-gap is selected, moving the tropical edge of the region of high values of  $\kappa_{\text{eff}}$  poleward (up to 25°S when waves with phase speeds between -10 and 10 m/s are removed). Note also the decrease in the maximal value of  $\kappa_{\text{eff}}$  in the surf zone for both filters. Our results are consistent with those of Bowman [1995, 1996] who suggested that the vortex-edge barrier is a result of the lack of waves with fast phase speeds comparable to the speed of the jet. Using simulations of the SKYHI general circulation model, Bowman and Hu [1997] further showed that mixing in the tropical lower stratosphere was controlled by waves propagating westward with phase speeds between -25 and -10 m/s, while removing all eastward-propagating waves reduced mixing in middle and high latitudes [see Bowman and Hu, 1997, Figures 10 and 14].

## 5. Summary and Conclusions

[21] In this study we reported on a specific numerical model capable of resolving scale issues, COMMID, which was developed by coupling two numerical models: MSDOL to simulate the stratospheric large-scale circulation in a realistic manner with forcing toward the reanalysis of NCEP below 100 hPa, and MIMOSA to describe the small-scale filamentary structures as produced by this large-scale circulation. To evaluate the performances of the model, we presented results for a particular event of tropical-air intrusion at midlatitudes across the southern subtropical barrier observed in July 2000.

[22] First, we verified from the comparison with a MIMOSA simulation driven by NCEP reanalyses, that the COMMID model was able to reproduce the pattern of the event thus accounting for the mechanisms, in spite of differences. Some of the differences may be explained by the differing background winds between MSDOL and NCEP. Also, because of the impact of gravity-wave drag on zonal-mean flow, more detailed studies should incorporate changes of the amplitude of the coefficients used in the gravity wave-drag parameterisation or the use of the Rayleigh friction. Another possibility is the lack of horizontal resolution of MSDOL. From this perspective, it should be

valuable to run MSDOL with a higher resolution (for example 2.5° in latitude by 5.625° in longitude) for more descriptive studies.

[23] Second, we made a detailed study of the contribution of each wave to the event. To do that, we changed the tropospheric wave forcing: COMMID was run with fields from NCEP filtered by zonal wave number and by phase speed. Thus one significant aspect of this study is that in it the tropospheric forcing was filtered rather than the actual stratospheric winds as done by Bowman [1996] and Bowman and Hu [1997]. Results from the contour advection calculations highlighted the major role played by wave 3. In addition, it was shown that the intrusion event did not occur in the absence of the slow eastward-propagating modes in the tropospheric forcing. Results from the effective diffusivity, on the other hand, showed that mixing was significantly reduced precisely at the locations where the phase speeds of the filtered waves were close to the speed of the mean zonal wind, in accordance with the results of Bowman [1996] and Bowman and Hu [1997]. What is important in this paper is that our results confirm the findings of previous studies, so they validate the use of our methodology based on the coupling of two models (that is an original approach) for studies of the isentropic transport in a dynamically consistent framework. The next step (that has already started) consists in using the COMMID model in a more general way for further investigations of the impact of the tropospheric circulation on the isentropic transport in the stratosphere for climate sensitivity purposes.

[24] **Acknowledgment.** The authors would like to thank the NOAA Climate Diagnostics Center (<http://www.cdc.noaa.gov/>) for providing portions of the NCEP data.

## References

- Andrews, D. G., J. R. Holton, and C. B. Leovy (1987), *Middle Atmosphere Dynamics, Int. Geophys. Ser.*, vol. 40, 489 pp., Elsevier, New York.
- Bencherif, H., et al. (2003), LIDAR observations of lower stratospheric aerosols over South Africa linked to large scale transport across the southern subtropical barrier, *J. Atmos. Sol. Terr. Phys.*, 65(6), 707–715.
- Bowman, K. P. (1995), Diffusive transport by breaking waves, *J. Atmos. Sci.*, 52(13), 2416–2427.
- Bowman, K. P. (1996), Rossby wave phase speeds and mixing barriers in the stratosphere: Part I. Observations, *J. Atmos. Sci.*, 53(6), 905–916.
- Bowman, K. P., and Y. Hu (1997), Tropical mixing barriers in the lower stratosphere in the Geophysical Fluid Dynamics Laboratory SKYHI model, *J. Geophys. Res.*, 102(D17), 21,465–21,478.
- Charney, J. G., and P. G. Drazin (1961), Propagation of planetary-scale disturbances from the lower into the upper atmosphere, *J. Geophys. Res.*, 66(1), 83–109.
- Chen, P., J. R. Holton, A. O'Neill, and R. Swinbank (1994), Isentropic mass exchange between the tropics and extratropics in the stratosphere, *J. Atmos. Sci.*, 51(20), 3006–3018.
- Fritts, D. C., and W. Lu (1993), Spectral estimates of gravity wave energy and momentum fluxes: Part II. Parameterization of wave forcing and variability, *J. Atmos. Sci.*, 50(22), 3695–3713.
- Hauchecorne, A., T. Peter, D. Balis, A. Gregman, M. P. Chipperfield, N. R. P. Harris, W. A. Norton, J. Staehelin, and M. Weber (2001), Mid-latitude and tropical ozone, in *European Commission—EUR 19867—European Research in the Stratosphere, 1996–2000: Advances in Our Understanding of the Ozone Layer During THESEO*, edited by G. T. Amanatidis and N. R. P. Harris, pp. 133–189, Eur. Comm., Luxembourg.
- Hauchecorne, A., S. Godin, M. Marchand, B. Heese, and C. Souprayen (2002), Quantification of the transport of chemical constituents from the polar vortex to midlatitudes in the lower stratosphere using the high-resolution advection model MIMOSA and effective diffusivity, *J. Geophys. Res.*, 107(D20), 8289, doi:10.1029/2001JD000491.
- Haynes, P. H. (2003), Critical layers, in *Encyclopedia of Atmospheric Science*, edited by J. R. Holton et al., pp. 582–589, Elsevier, New York.

- Haynes, P., and E. Shuckburgh (2000), Effective diffusivity as a diagnostic of atmospheric transport: 1. Stratosphere, *J. Geophys. Res.*, *105*(D18), 22,777–22,794.
- Lott, F., L. Fairhead, F. Hourdin, and P. Levan (2005), The stratospheric version of LMDz: Dynamical climatologies, arctic oscillation, and impact on the surface climate, *Clim. Dyn.*, in press.
- McIntyre, M. E., and T. N. Palmer (1984), The “surf zone” in the stratosphere, *J. Atmos. Terr. Phys.*, *46*(9), 825–849.
- Methven, J., and B. Hoskins (1999), The advection of high-resolution tracers by low-resolution winds, *J. Atmos. Sci.*, *56*(18), 3262–3285.
- Morel, B., P. Keckhut, H. Bencherif, A. Hauchecorne, G. Mégie, and S. Baldy (2004), Investigation of the tidal variations in a 3-D dynamics-chemistry-transport model of the middle atmosphere, *J. Atmos. Sol. Terr. Phys.*, *66*(3–4), 251–265.
- Nakamura, N. (1996), Two-dimensional mixing, edge formation, and permeability diagnosed in an area coordinate, *J. Atmos. Sci.*, *53*(11), 1524–1537.
- Nakamura, N., and J. Ma (1997), Modified Lagrangian-mean diagnostics of the stratospheric polar vortices: 2. Nitrous oxide and seasonal barrier migration in the cryogenic limb array etalon spectrometer data and SKYHI general circulation model, *J. Geophys. Res.*, *102*(D22), 25,721–25,735.
- Plumb, R. A. (2002), Stratospheric transport, *J. Meteorol. Soc. Jpn.*, *80*, 793–809.
- Polvani, L. M., and R. Saravanan (2000), The three-dimensional structure of breaking Rossby waves in the polar wintertime stratosphere, *J. Atmos. Sci.*, *57*(21), 3663–3685.
- Portafaix, T., B. Morel, H. Bencherif, S. Baldy, S. Godin-Beekmann, and A. Hauchecorne (2003), Fine-scale study of a thick stratospheric ozone lamina at the edge of the southern subtropical barrier, *J. Geophys. Res.*, *108*(D6), 4196, doi:10.1029/2002JD002741.
- Randel, W. J., J. C. Gille, A. E. Roche, J. B. Kumer, J. L. Mergenthaler, J. W. Waters, E. F. Fishbein, and W. A. Lahoz (1993), Stratospheric transport from the tropics to middle latitudes by planetary-wave mixing, *Nature*, *365*(6446), 533–537.
- Rose, K., and G. Brasseur (1989), A three-dimensional model of chemically active trace species in the middle atmosphere during disturbed winter conditions, *J. Geophys. Res.*, *94*(D13), 16,387–16,403.
- Rosenlof, K. H., A. F. Tuck, K. K. Kelly, J. M. Russell III, and H. P. McCormick (1997), Hemispheric asymmetries in water vapor and inferences about transport in the lower stratosphere, *J. Geophys. Res.*, *102*(D11), 13,213–13,234.
- Stewartson, K. (1978), The evolution of the critical layer of a Rossby wave, *Geophys. Astrophys. Fluid Dyn.*, *9*(3–4), 185–200.
- U.N. Environment Programme/World Meteorological Organization (UNEP/WMO) (2002), Scientific assessment of ozone depletion: 2002, *Rep. 47*, WMO Global Ozone Res. and Monit. Project, Geneva.
- Warn, T., and H. Warn (1978), The evolution of a nonlinear critical level, *Stud. Appl. Math.*, *59*(1), 37–71.
- Waugh, D. W., et al. (1994a), Transport out of the lower stratospheric Arctic vortex by Rossby wave breaking, *J. Geophys. Res.*, *99*(D1), 1071–1088.
- Waugh, D. W., R. A. Plumb, P. A. Newman, M. R. Schoeberl, L. R. Lait, M. Loewenstein, J. R. Podolske, J. W. Elkins, and K. R. Chan (1994b), Fine-scale, poleward transport of tropical air during AASE 2, *Geophys. Res. Lett.*, *21*(23), 2603–2606.

---

S. Baldy, H. Bencherif, B. Morel, and T. Portafaix, Laboratoire de Physique de l'Atmosphère, Université de La Réunion, 15 avenue René Cassin, B.P. 7151, Saint-Denis Messag., Cedex 9, F-97715 La Réunion, France. (beatrice.morel@univ-reunion.fr)

A. Hauchecorne and P. Keckhut, Service d'Aéronomie, Institut Pierre-Simon Laplace–CNRS, B.P. 3, F-91371 Verrières-le Buisson, France.